Lumped-Parameter Equivalent Circuit Modeling of CMUT Array Elements

Tony Merrien, Audren Boulmé, Dominique Certon

IEEE Open Journal of
Ultrasonics, Ferroelectrics, and Frequency Control

Received 4 November 2021; accepted 8 December 2021.
Date of publication 20 December 2021; date of current version 7 January 2022.

Digital Object Identifier 10.1109/OJUFFC.2021.3134938

Lumped-Parameter Equivalent Circuit Modeling of CMUT Array Elements

TONY MERRIEN[1,2], AUDREN BOULMÉ[2], AND DOMINIQUE CERTON[1], (Member, IEEE)

[1]GREMAN UMR-CNRS 7347, University of Tours, 37071 Tours, France
[2]MODULEUS SAS, 37100 Tours, France

CORRESPONDING AUTHOR: D. CERTON (dominique.certon@univ-tours.fr)

ABSTRACT Design and modeling are key steps in the value chain of Capacitive Micromachined Ultrasonic Transducer (CMUT) arrays. Although CMUT array element models are very powerful, most of them are still limited in their use as tools for electronic design assistance. The electroacoustic equivalent circuits developed are mainly based on a distributed-element approach while lumped-parameter electrical circuits are better suited for electronic software design tools interoperations. To meet this need, the present study aims to implement an electroacoustic equivalent scheme of a full array element, based on a two-port network representation made of lumped-parameters. After an extensive bibliographical review of CMUT models, the new model is set-up from a fully distributed approach using Foldy's electroacoustic definitions at the element level. Transmit and receive modes are implemented using scalar equations given by the lumped parameters. Moreover, based on a reciprocity analysis, the performance of the complete measurement chain in emission and reception will be defined using the relevant transfer functions. Finally, to help one design CMUT array elements for a given application, a method based on the computation of membranes thickness-size master curves is proposed. The two-port network representation of a full CMUT-based array element allowed by the new lumped-parameter modeling opens a wide range of possibilities regarding array design, electronic integration, operations with acoustic propagation simulation tools and more.

INDEX TERMS Capacitive micromachined ultrasonic transducers, MEMS, finite-difference, lumped-element, reciprocity, design, electroacoustics.

I. INTRODUCTION

AFTER years of innovative development [1]–[4], Capacitive Micromachined Ultrasonic Transducers (CMUTs) are now a mature technology that can address a wide range of applications, ranging from ultrasonic medical imaging [5], [6] to gas sensors [7], [8]. CMUT fabrication processes have greatly improved in terms of robustness and reproducibility, while a large choice of electronic circuit architectures [9]–[11] are also available to drive these ultrasonic arrays efficiently. Transducer modeling followed the same evolution, and many approaches were proposed in the literature to help one design CMUTs according to the targeted application. Although commercial finite element-based tools are well suited for the simulation of these devices, many authors have proposed other approaches. The primary objective of these works was to significantly reduce calculation costs (*i.e.,* time and memory volume required), and to develop design tools for ultrasonic transducers which can be easily connected to electronic circuit simulators (*e.g.,* LTspice, Simulink, etc.). Because CMUT-based ultrasonic arrays design requires a very large number of input parameters, it is often mandatory to use dedicated simulation tools. To facilitate the inventory of all input/output parameters required to design a CMUT probe, three analysis scales should be considered. The first is the unit cell scale: geometry and thickness of materials. The second is the ultrasonic emitter/receiver element scale: number of cells, pitch between cells, choice of cells dimensions (*e.g.,* multi-frequency devices [12]). The third is the whole array scale: geometry of elements, layout of elements and inter-element crosstalk. Note that Piezoelectric Micromachined Ultrasonic Transducers (PMUTs) can also exhibit the same complexity [13], [14]. This paper is in line with these modeling efforts and focuses on the development of an accurate multi-element

CMUT-based array model that associates only two electrical degrees of freedom and two acoustic degrees of freedom to each emitter/receiver element.

Using a one dimensional (1-D) equivalent piston model to simulate a unit CMUT cell has been widely demonstrated, approved and is very often used as it simplifies the change of scale from the unit cell to the ultrasonic transmitter element [15]–[18]. Moreover, nonlinear effects due to large excitation voltages used to drive CMUTs are easier to consider with 1-D equivalent piston models [19]–[22]. However, the equivalent piston model of the unit cell must be implemented with great care since the fluid coupling strongly affects the mechanical behavior of the moving plate. For instance, using Mason's approach is only reliable at low frequencies [23]. This method relies on the separate computation of the self-mechanical impedance and the self-radiation impedance of the CMUT cell but does not enable the high mechanical cut-off frequency (*i.e.,* the second antisymmetric vibration mode) to be considered. To overcome this issue, two approaches are currently used. The first is to compute the response of a CMUT cell acoustically loaded [24], [25] with a finite element [26], [27] or finite difference model [28] in order to extract the equivalent piston model parameters using Foldy's definition [29]. The second approach is achieved using the general analytical mathematical expression of the plate behavior loaded with a fluid. Then, the correct parameters of this mathematical expression according to the boundary conditions lead to the final solution. This approach is interesting since it avoids heavy numerical computations, if a valid analytical expression of the plate displacement is provided [30].

At the emitter/receiver element scale, up to hundreds of cells can make up a full element so one can get a suitable active surface needed to deliver the required pressure in the medium and perform ultrasound imaging. In this case, to compute the electroacoustic response of the transducer both in emission and reception, mutual acoustic interactions (*i.e.*, mutual acoustic impedances [31]) between each cell has to be determined in the frequency range of interest. Mutual coupling was proven to have a non-negligible effect on the array performance, resulting in additional forces and visible crosstalk effects (*i.e.*, the baffle mode) [32]. Exact expressions of mutual interactions between cells are well known [33], [34] but can be extremely time consuming to compute. Shieh *et al.* [35] developed a method to improve computation time by setting different scales of acoustic coupling based on the ratio between the acoustic wavelength and the cell-to-cell distance. In addition, Oguz *et al.* [36] have proposed a tenth order polynomial approximation of Porter's exact equation [34] while Maadi and Zemp [12] have approximated the equation as a function of edges conditions by neglecting high order terms. The mutual acoustic impedances computed are then used to construct the boundary element matrix [37]–[39] that introduces the transducer/fluid coupling in the set of equations governing the element behavior. Even if very fast and efficient, this matrix representation is heavy to manipulate when the electroacoustic performance in emission, reception or emission/reception modes must be computed. The degrees of freedom number can be very large since it corresponds to the number of CMUT cells per element. Hence, it is difficult to interoperate with ultrasonic imaging simulation tools (*e.g.*, Field II [40], DREAM [41]) since they require only one input data (*i.e.*, the spatial mean particular velocity). Moreover, for the electronic driving circuits design, the use of equivalent lumped-parameter model is clearly more suitable than the use of distributed-element models. In a more global context, the use of lumped-parameter models (*i.e.*, equivalent two-port-network models) allow a greater insight into the simulation results and their exploitation.

The aim of this paper is to show that it is still possible to reduce the degrees of freedom number by replacing the element with a single ultrasonic source, modeled as an electrical two-port network. This paper follows the work presented by Caronti *et al.* [24] and extended by Savoia *et al.* [27] where an equivalent two-port network of a CMUT-based ultrasonic emitter was computed from finite element simulations. In the present case, the computations started from the set of matrix relations previously presented by Meynier *et al.* [25]. Furthermore, the distributed-element model which serves as a basis for the development of the lumped-parameter model, was validated experimentally [38]. Therefore, this paper will focus on theoretical developments without presenting experimental results. The developed model does not consider the nonlinearity of CMUTs. Many authors have proposed approaches that could be applied to introduce nonlinearity phenomena in the presented model [3], [17], [21], [27], [42]. However, this issue is out of the scope of this paper and will not be addressed.

This paper is organized as follows: the first section is dedicated to the two-port network model implementation. It starts with a summary of the equations that govern the CMUT/fluid coupling expressed with the boundary element matrix, so called afterwards the distributed-element model. Then, the lumped-element parameters of the equivalent two-port/four parameters network of one element is described. Foldy's analysis will be used to define which acoustic variables are kept while the simulation scale is changed from the distributed-element model to the lumped-parameter model.

The second section gathers a set of simulation results and discussions to address three specific points. First, the pressure fields obtained with both models is compared to assess the validity limits of the lumped-parameter element scale approach and discuss its applicability with different beamforming strategies. Then, a discussion is engaged on mutual interactions and their impact on the electroacoustic response of a single column of CMUTs. It is shown that, thanks to the lumped-parameter representation of the array element, the mutual acoustic interactions can be modelled through a reduced degrees of freedom and computational efficient acoustic impedance term. Finally, according to the application targeted, the two-port network model transfer function optimization is discussed. Based on Schmerr *et al.* analysis [43], this work provides transfer functions combinations

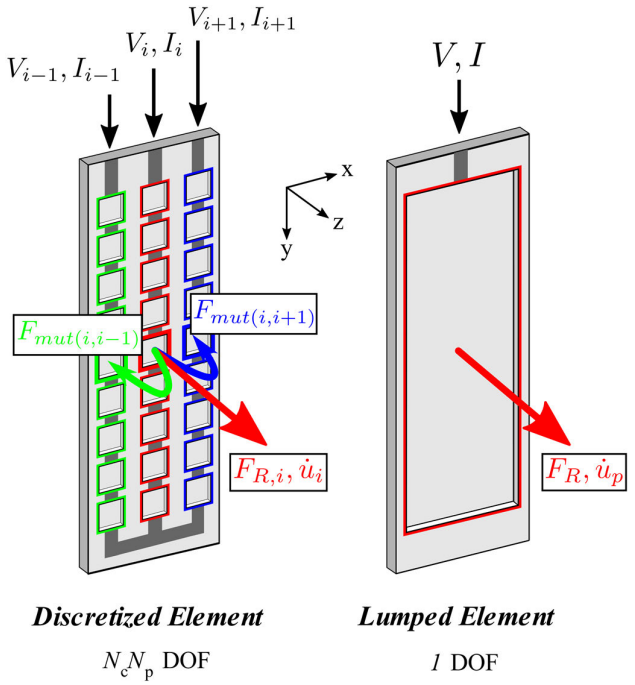

FIGURE 1. **Sketch of a CMUT-based array element made with a finite number of cells and its lumped equivalent piston representation. The number of degrees of freedom (DOF) is reduced from a great number of cells (N_c x N_p) to only one, which enables the multiple cell element to be represented by a two-port network.**

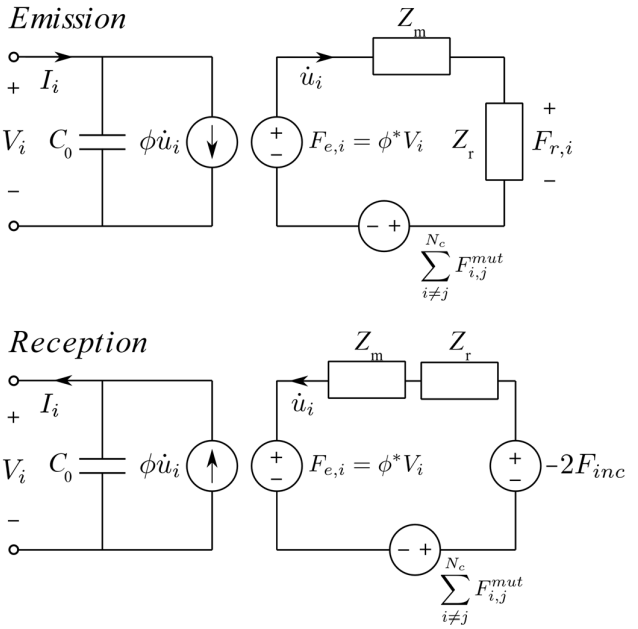

FIGURE 2. **Equivalent circuit of one CMUT cell with 1-D periodic boundary conditions in emission and reception.**

in emission and reception that meet the electroacoustic reciprocity theorem.

The last section is a practical exploitation of the lumped-parameter array element model that helps design an array element, focused on building design rules and charts for a given application. The acoustic design of a $5MHz$ centered element and $\lambda/2$ pitch array aimed at general ultrasound imaging purposes is used as an illustrative example. CMUT topology and materials will be defined in agreement with the standard wafer bonding process [44].

II. MODEL SET UP

This first section aims to introduce the theory behind the lumped-parameter array elements equivalent circuit modeling and demonstrate its associated equations. A sketch of the intended result is presented Fig. 1. The section starts with a brief reminder of the distributed-element input/output relationships for a 1-D linear array element. Then, based on Foldy's analysis, the Section II.B focuses on the lumped-parameter model implementation.

A. DISTRIBUTED-ELEMENT MODEL

At the array element scale, each CMUT cell can be modeled as a single piston source, with an equivalent electroacoustic circuit presented in emission and reception modes Fig. 2. This equivalent circuit contains four main parameters: the electrical capacitance C_0, the electrical-to-acoustic transformation ratio ϕ, the mechanical impedance Z_m and the self-radiation impedance Z_r. Each of these parameters depend on the CMUT biasing voltage and can be obtained using the distributed model to resolve the discretized governing equations of the transducer. The same representation exists for PMUT cells [45], [46]. It is worth reminding that the equivalent piston model, which is widely admitted by the scientific community, is suitable for predicting the average velocity of the CMUT plate and has been validated in previous works [25]. The main limitation of this model lies within the radiated pressure field directivity prediction. The two models are perfectly matched if the size of the CMUT is small compared to the acoustic wavelength. For ultrasound imaging applications, this condition is met since the element width is always smaller than the wavelength. For the remaining sections of this paper, the latter assumption is considered valid.

In the array element case (cf. Fig. 2), Boulmé and Certon [38] took into consideration the element aspect ratio (*i.e.*, high elevation to width ratio) to reduce the degrees of freedom to one CMUT cell per column. For simplicity, this consideration is kept throughout this paper. It was assumed that each cell inside one column sees the same radiating boundary conditions (*i.e.*, 1-D periodic boundary conditions). The self-radiation impedance of CMUTs with 1-D radiating periodic conditions is denoted Z_r. The electrical inputs of the CMUT equivalent circuit are the applied voltage V_i and the entering electrical current I_i. The acoustic outputs are the radiated acoustic force $F_{r,i}$ and the spatial mean acoustic velocity over one cell denoted $\dot{u}_i$. Here, i is an integer that ranges from 1 to N_c, the number of columns in the array element. Finally, inter-cell crosstalk is introduced for the i^{th} column by the mutual interaction force $F_{i,j}^{mut}$ where j is an integer that ranges from 1 to N_c and denotes the array element columns with respect to $j \neq i$.

The set of equations that govern the collective behavior of CMUT cells yields under matrix form:

$$\begin{cases} [I] = j\omega N_p C_0 [V] + N_p \phi [\dot{u}] \\ [F_r] = \phi^* [V] - Z_m [\dot{u}] \\ [F_r] = \left[K_{fluid}\right] [\dot{u}] \end{cases} \tag{1}$$

$[I]$, $[V]$, $[\dot{u}]$ and $[F_R]$ are vectors with dimension N_c that gather electrical current, voltage, mean velocity, and radiated force values, respectively. N_p is the number of CMUT cells per column in the array element. The boundary matrix $\left[K_{fluid}\right]$ is written:

$$\left[K_{fluid}\right] = \begin{bmatrix} Z_r & Z_{1,2}^{mut} & \dots & Z_{1,N_c}^{mut} \\ Z_{2,1}^{mut} & Z_r & \dots & \vdots \\ \vdots & \vdots & \ddots & Z_{N_c-1,N_c}^{mut} \\ Z_{N_c,1}^{mut} & \dots & Z_{N_c,N_c-1}^{mut} & Z_r \end{bmatrix} \tag{2}$$

where the diagonal term is the self-radiation impedance Z_r of a single CMUT cell with 1-D periodic boundary conditions and the off-diagonal term $Z_{i,j}^{mut}$ is the mutual impedance between one CMUT cell of the i^{th}column and the j^{th}column in 1-D periodic conditions.

When a CMUT array element works as a receiver, the problem to be solved is slightly different. One has to compute the delivered output voltage and electrical current produced by incoming ultrasonic waves that impinge the transducer's front face. In order to mathematically formulate the problem, an incident wave with amplitude $F_{inc,i}$ $(i = 1, \dots, N_c)$ is introduced for each cell on the acoustical port side. In practice, it can be assumed that the incident wave is a plane wave when it reaches the front face of the CMUT transducer. This is of course a strong hypothesis, but this assumption is often accepted as being correct in practice without reducing the relevance of the model [20]. In this case, each cell sees the same incident acoustic force F_{inc}. To compute the electrical response of one element, the problem has to be reformulated in order to model the incident acoustic wave as a force generator that is linked to the governing equations of the CMUTs. This problem was already discussed and solved by L. Foldy ([29], Equation 11). Foldy shows the equivalent force generator is made of a force source, so-called blocked force, in series with the radiation impedance of the receiver. The force source is called the blocked force since it corresponds to the force applied to the receiver when its front face is blocked (*i.e.*, the particular velocity is null). The blocked force is the sum of the incident force and the force linked to the scattered pressure by the receiver. In the case of an imaging array, the transducer surface is far larger than the acoustic wavelength and the incident wave follows a total reflection when it impinges its front face ([31], Paragraph 6.6). Hence, the reflected wave is exactly the same as the incident wave, and the blocked forced F_B is twice the incident wave such that $F_B = 2F_{inc}$.

The sign conventions of variables (F_{inc} is negative) were changed to be consistent with the reception process. Hence, the particle velocity is set to be directed inward from the transducer surface and the current is reversed. The matrix relations become:

$$\begin{cases} [I] = -j\omega N_p C_0 [V] + N_p \phi [\dot{u}] \\ -2 [F_{inc}] - \left[K_{fluid}\right] [\dot{u}] = \phi^* [V] + Z_m [\dot{u}] \end{cases} \tag{3}$$

$[F_{inc}]$ is a diagonal matrix containing the uniform incident force. Note that the incident acoustic pressure wave P_{inc} is straightforward, corresponding to the incident acoustic force simply multiplied by the CMUT cell surface. The left hand side of the second equation is the same expression described by Foldy [29] that takes into account the transmitted, reflected and diffracted pressure by the transducer.

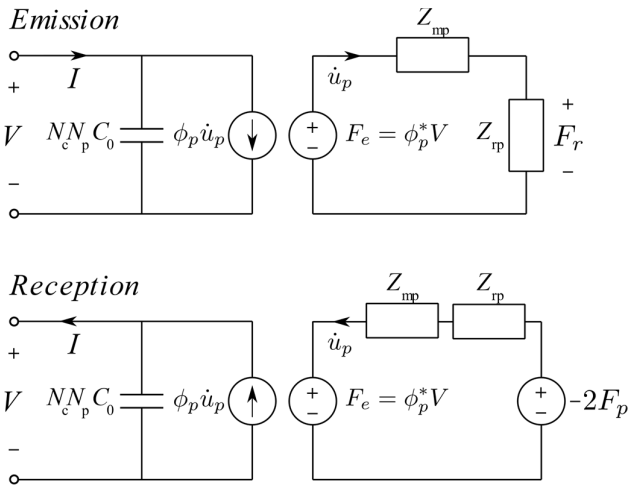

FIGURE 3. Lumped-parameter electrical circuit for a CMUT array element in emission and reception modes.

B. EQUIVALENT LUMPED-PARAMETER MODEL

The first step to implement a lumped-parameter model of a full array element (cf. Fig. 3) is to define new physical variables of an equivalent piston that ensure continuity with the distributed-element model. These variables are computed at least once with the distributed-element model to get a solution of the displacement field vector $[\dot{u}_s]$.

As proposed by Foldy [29], it is chosen to keep the acoustic flow rate and the total acoustic power (*i.e.,* the radiated and mechanical part) of the acoustic port. Since all CMUT columns are electrically connected in parallel, the voltage V on the electrical port is the same for each column and the electrical current I becomes the summation of each column's current. To preserve the flow rate and because a part of the element is acoustically inactive, the output spatial mean velocity of the equivalent piston $\dot{u}_p$ must be normalized by the ratio of the active area and the element area. This yield, using the specific solution $[\dot{u}_s]$:

$$\dot{u}_p = N_p \frac{S_{mut}}{S_p} \sum_{i=1}^{N_c} \dot{u}_{s,i} \tag{4}$$

where S_{mut} is the active surface of one CMUT cell, S_p is the total surface of one element and $\dot{u}_{s,i}$ are the component of the displacement field vector $[\dot{u}_s]$.

The mean radiated and mechanical power conservation following Foldy's definition [29], enables the element equivalent mechanical and radiation impedances computation, respectively Z_{mp} and Z_{rp}:

$$\begin{cases} Z_{mp} = \dfrac{2W_m(\omega)}{\left|\dot{u}_p\right|^2} \\ Z_{rp} = \dfrac{2W_r(\omega)}{\left|\dot{u}_p\right|^2} \end{cases} \tag{5}$$

$W_r(\omega)$ is the radiated acoustic power and $W_m(\omega)$ is the power absorbed by the CMUT. Their mathematical expressions are given by the following relationships:

$$\begin{cases} W_m(\omega) = \dfrac{1}{2} N_p \left[\dot{u}_s\right]^{T*} \left[K_m\right] \left[\dot{u}_s\right] \\ W_r(\omega) = \dfrac{1}{2} N_p \left[\dot{u}_s\right]^{T*} \left[K_{fluid}\right] \left[\dot{u}_s\right] \end{cases} \tag{6}$$

where $[\ ]^{T*}$ stands for the transposed complex conjugate matrix and $[K_m]$ is the diagonal matrix of the mechanical impedance Z_m. From the distributed-element model relationships (1), the variables Z_{mp}, Z_{rp} and $\dot{u}_p$ are introduced after a few mathematical manipulations. Because all columns of an element are electrically connected in parallel, they have the same voltage V_i. From the first relation of (1) that links the current to the voltage, a summation over each current vector components leads to the following relation:

$$\begin{aligned} I &= j\omega N_p C_0 \sum_{i=1}^{N_c} V_i + N_p \phi \sum_{i=1}^{N_c} \dot{u}_{s,i} \\ I &= j\omega N_p N_c C_0 V + \phi_p \dot{u}_p \end{aligned} \tag{7}$$

Here, I is the total input current and $\phi_p = \frac{S_p}{S_{mut}}\phi$ is the new electroacoustic transformation coefficient of the equivalent piston.

If one multiplies the left and right side of the second and third relations of (1) by the complex transposed vector $[\dot{u}_s]^{T*}$, the following expression is obtained:

$$\begin{aligned} \left[\dot{u}_s\right]^{T*} \left(\left[K_{fluid}\right] + \left[K_m\right]\right) \left[\dot{u}_s\right] &= \phi^* V \sum_{i=1}^{N_c} \dot{u}^*_{s,i} \\ \frac{Z_{rp}}{N_p} \left|\dot{u}_p\right|^2 + \frac{Z_{mp}}{N_p} \left|\dot{u}_p\right|^2 &= \phi^* V \frac{S_p}{N_p S_{mut}} \dot{u}^*_p \\ \left(Z_{rp} + Z_{mp}\right) \dot{u}_p &= \phi^*_p V \end{aligned} \tag{8}$$

It may be noted at this point that multiplying each side of second and third relations of (1) (*i.e.*, Newton's second law) by $[\dot{u}_s]^{T*}$, gives the energy balance equation of the system. Using these results, one can establish the equivalent circuit of the new equivalent piston as presented Fig. 3. Hence, in transmit mode the output acoustic data of a CMUT array element (*i.e.,* the particle velocity $\dot{u}_p$ and the radiated force F_r) are obtained through the following relationships:

$$\begin{cases} I = j\omega N_p N_c C_0 V + \dfrac{\left|\phi_p\right|^2}{Z_{mp} + Z_{rp}} V \\ F_r = \phi^*_p V - Z_{mp} \dot{u}_p \\ F_r = Z_{rp} \dot{u}_p \end{cases} \tag{9}$$

In reception the problem is reversed, the input is either the flow rate $\dot{u}_p$ or the acoustic force F_r and the outputs are the electrical current I and/or the delivered voltage V. The current in (7) is reversed and the particular velocity $\dot{u}_p$ is set to be directed inward from the transducer surface, which yields:

$$I = -j\omega N_p N_c C_0 V + \phi_p \dot{u}_p \tag{10}$$

Again, if one assumes that the incident wave is a plane wave, the incident acoustic force vector $[F_{inc}]$ is therefore uniform. The complex transposed vector $[\dot{u}_s]^{T*}$ is multiplied at each side of the second relation of (3) to introduce the reversed energy balance equation:

$$\begin{aligned} -2F_{inc} \left[\dot{u}_s\right]^{T*} - \left[\dot{u}_s\right]^{T*} \left[K_{fluid}\right] \left[\dot{u}_s\right] - \left[\dot{u}_s\right]^{T*} \left[K_m\right] \left[\dot{u}_s\right] \\ = \phi^* \left[\dot{u}_s\right]^{T*} \left[V\right] \end{aligned} \tag{11}$$

which can be further reduced to the scalar expression:

$$\begin{aligned} -2F_{inc} \sum_{i=1}^{N_c} \dot{u}^*_{s,i} - \frac{Z_{rp}}{N_p} \left|\dot{u}_p\right|^2 - \frac{Z_{mp}}{N_p} \left|\dot{u}_p\right|^2 = \phi^* V \sum_{i=1}^{N_c} \dot{u}^*_{s,i} \\ -2F_p - \dot{u}_p \left(Z_{mp} + Z_{rp}\right) = \phi^*_p V \end{aligned} \tag{12}$$

F_p represents the incident acoustic force applied to the surface of the element and defined by:

$$F_p = \frac{S_p}{S_{mut}} F_{inc} \tag{13}$$

It is worth emphasizing that the acoustic impedance terms appearing are the same for both emission and reception modes after multiplying by $[\dot{u}_s]^{T*}$ since the set of equations represents the energy balance of the system. The electrical admittance is directly obtained with the lumped-parameter model (cf. Fig. 3):

$$Y_{elec} = j\omega N_p N_c C_0 + \frac{\left|\phi_p\right|^2}{Z_{mp} + Z_{rp}} \tag{14}$$

Meynier *et al.* [25] obtained another scalar expression for the electrical admittance, based on the distributed-element model equations:

$$Y_{elec} = j\omega N_p N_c C_0 + N_p N_c \left|\phi\right|^2 \sum_{k=1}^{N_c} \sum_{l=1}^{N_c} Y_{kl} \tag{15}$$

Here, Y_{kl} are the admittance matrix terms: $[Y] = \left(\left[K_{fluid}\right] + \left[Z_m\right]\right)^{-1}$. The lumped-parameter and distributed element gives naturally the same result, which emphasizes the theoretical validity of our new equivalent piston definition.

To summarize this first section, it is important to remember that the equivalent lumped-parameter circuit of one array element is constructed to ensure continuity with the

distributed-element model through four global variables: the input electrical current I, the voltage V, the acoustic flow rate $S_p\dot{u}_p$ and the total acoustic power $W_r + W_m$ (radiated and non-radiated). This means that the output force, and consequently the pressure, given by the lumped-parameter circuit cannot be used directly. Before pressure field computations using the classical Rayleigh's integral, it is recommended to use $\dot{u}_p$ as a flat piston source condition with the element geometry. This nuance is essential and motivates the validation step of the pressure field calculation in the next section. On the other hand, it also implies that every electrical-to-acoustic transfer function produced by the model cannot be directly exploited and should therefore be carefully identified (cf. Section III.C). Finally, even if out of the scope of this paper, one can include additional components in the equivalent circuit such as parasitic capacitance, dielectric losses, electrode input resistance, etc.

III. SIMULATION RESULTS AND DISCUSSIONS

The first part of this section aims to compare the predicted pressure field between the distributed-element model described in Section II.A and the lumped-parameter model described in Section II.B. Because of cells non-discretization and the new equivalent piston definition, the first task is to ensure the validity of the model. To do so, we evaluate at which propagating distance the distributed-element model and the lumped-parameter model provide equal pressure fields. To further demonstrate the validity of the lumped-parameter model, the study is extended by adding neighboring elements to assess the impact of mutual interaction effects on the response of an isolated single element. Two beamforming strategies will be considered, the method for which the emitted pressure field is focused and a plane wave imaging strategy. Firstly, the response of an isolated single element is compared with the response of a single element surrounded on each side by 8 inactive elements of the same geometry. Then, the case of single element surrounded by 16 active elements in an array is considered. For a plane wave emitted at a 0° angle, this corresponds to a limit case for the proposed lumped-parameter model since all elements are excited at the same time without delay between each other.

The Section III.B shows how to easily obtain the equivalent acoustic radiation impedance term Z_{rp} without solving the set of the distributed-element model equations. The method relies on the separation of the acoustic radiation impedance as the sum of two impedances, one that models the response of a CMUT array element coupled to a fluid medium without mutual coupling effects (as if $Z_{i,j}^{mut} = 0$ in (2)), and one that models only the mutual acoustic effects (as if $Z_r = 0$ in (2)).

Finally, based on the reciprocity analysis proposed by Schmerr and Song [43], two transfer functions (acoustical-to-electrical and electrical-to-acoustical) are examined. Based on these definitions, we seek to optimize the performances of a CMUT-based array element used in a classical pulse-echo imaging setup.

TABLE 1. Dimensions of the CMUT and physical properties of materials used for simulation. Membrane is made of a silicon (Si) layer and an aluminum (Al) electrode layer.

Layer	Gap (Vacuum)	Membrane (Si)	Electrode (Al)
Thickness [nm]	100	950	50
Width [µm]	n/a	30	30
Young's Modulus [GPa]	n/a	128	68
Poisson coefficient	n/a	0.22	0.35
Density [kg/m^{-3}]	n/a	2330	2700
Relative permittivity	1	3.9	n/a

A. MODEL VALIDATION THROUGH TRANSMITTED PRESSURE ANALYSIS

This part focuses on the model validation and aims to clearly define the conditions for which the equivalent lumped-parameter model can be used and considered accurate enough for array performance predictions. To lead this work, a realistic case, namely the simulation of an array made of square shape CMUT cells, was used as an illustration. The design parameters are described in Table 1. The CMUT plate is made of a silicon layer covered with an aluminum electrode. The membranes size is $30\mu m \times 30\mu m$, the element is $6.5mm$ long and $100\mu m$ wide. The full element is comprised of 3 columns, 198 lines and a CMUT-to-CMUT kerf of $3\mu m$. This value is consistent with standard performances of wafer bonding process [47], [48]. This design gives a collapse voltage of $V_C = 29V$ and immersed velocity central frequency of $f = 4MHz$ in water ($\rho = 1000kg/m^3$ and $c_0 = 1500m/s$).

The membrane velocity obtained for a biasing voltage of $V_{DC} = 23V$ is presented Fig. 4. The computed output spatial mean velocity of the transducer shows a bandwidth of 102% and a high cut-off frequency (*i.e.*, the mechanical cut-off frequency of the CMUT) at $26.6MHz$. The mode observed at $5MHz$ (so-called baffle mode) is due to crosstalk phenomena where neighboring CMUT cells are vibrating out-off phase [24], [32], [37]. As explained by Ronnekleiv [49], due to viscoelastic effects, these modes are strongly attenuated when the array is encapsulated with a passivation layer [50]. In practice, it does not appear in the emitted pressure field and remains only a mean contribution that corresponds to a situation where all the cells are vibrating in-phase [23]. More recently, our group showed that these modes disappear from the electroacoustic response of CMUT arrays encapsulated with viscoelastic materials [51]. In the next paragraph, it will be shown how these parasitic modes can be suppressed from the simulations using the lumped-parameter model without losing any accuracy and even facilitating the array element performance computation (*i.e.*, bandwidth and central frequency).

To compute the pressure field, the toolbox DREAM (Discrete REpresentation Array Modeling) [41] was used in a MATLAB environment. This toolbox can be used to compute the diffraction impulse response for any geometry and

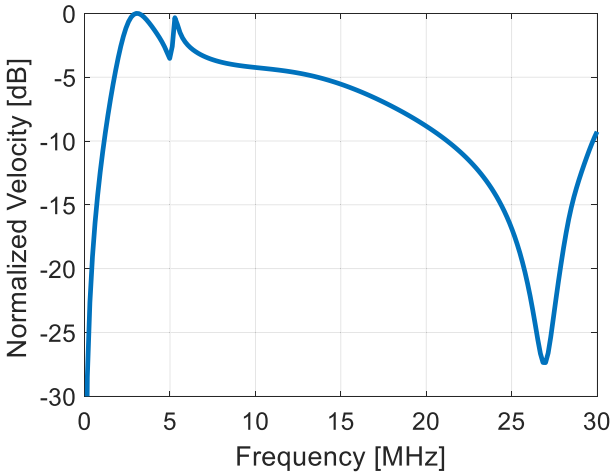

FIGURE 4. Spatial mean output particular velocity of the CMUT-based array element described in Table 1 at a biasing voltage of 23 V, with a 1*V* excitation voltage and normalized by its maximum value of 18 mm/s.

source conditions. Here, rigid baffle radiating boundary conditions were used to be consistent with the output velocity source condition provided by the lumped-parameter and the distributed-element models. The simulated pressure fields spectra are depicted Fig. 5 for two distances, at $0.01mm$ and $1mm$ from the emitter with an excitation voltage of one volt. The central frequency shifts to higher frequencies due to diffraction effects, and the bandwidth is increased. However, this result must be considered with great care since the medium attenuation was not considered (this point is out of the focus of this paper).

The crosstalk mode at $5MHz$ mode remains because encapsulation layer and viscoelastic effects were not considered. The most important result to highlight is the comparison between the two models. Near the transmitter at $0.01mm$, the lumped-parameter equivalent model fails to perfectly match the distributed-element approach. However, both models converge very quickly as their results are equal at $1mm$ of propagation distance. This distance corresponds to only a few acoustic wavelengths and greater propagation distances naturally induce correct results. This result is consistent with a basic principle of waves propagation which states that any radiating surface can be decomposed as a sum of source points. In this case, CMUTs play this role since, on one hand, they are modelled as perfectly rigid flat pistons (cf. Section II.A), and on the other hand, their size is small compared to the acoustic wavelengths covered by the emitted acoustic pulse. The non-discretization of each cell that make up the entire element leads to an incorrect evaluation of the near field pressure at submillimeter distances. This is the main drawback of the array element lumped-parameter model. In a practical case, encapsulation of the array with a $1mm$ thin polymer layer ensures that the lumped-parameter approach remains suitable for ultrasound imaging applications.

To extend the validity of the lumped-parameter model, the comparison is made for elements with higher number of

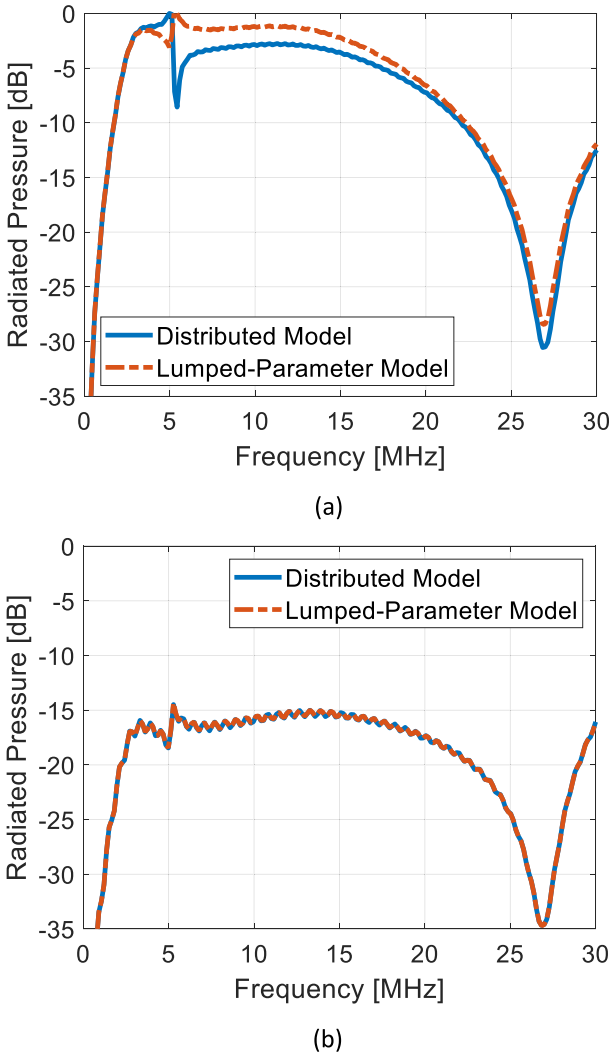

FIGURE 5. Output pressure simulation results of a CMUT array element obtained for $V_{DC} = 0.8V_C$. The first graph (a) shows the radiated pressure spectrum at $0.01mm$ and stress the differences with both approaches linked to the non-discretization of each cell in the very close field. The second graph (b) shows the radiated pressure spectrum at $1mm$ and illustrate the quick convergence of both models towards the same result. All curves are normalized by the maximum radiated pressure value $24kPa$ obtained with a 1*V* excitation voltage.

columns and the same CMUT-to-CMUT pitch. Of course, the larger is the element size, the greater the distance at which the two models are superposed. The mean absolute error between the two models is plotted in Fig. 6. As expected, the error is greater at very small distances but both models converge independently from their architectures towards zero after a few propagation wavelengths.

As outlined in introduction of this section, to further evaluate the limits of the newly proposed model, two additional cases were considered. In the remaining paragraphs of this section, the inter-element kerf is set to $15\mu m$, in line with standard design values and microfabrication capabilities. For the first, an acoustic aperture comprised of one excited

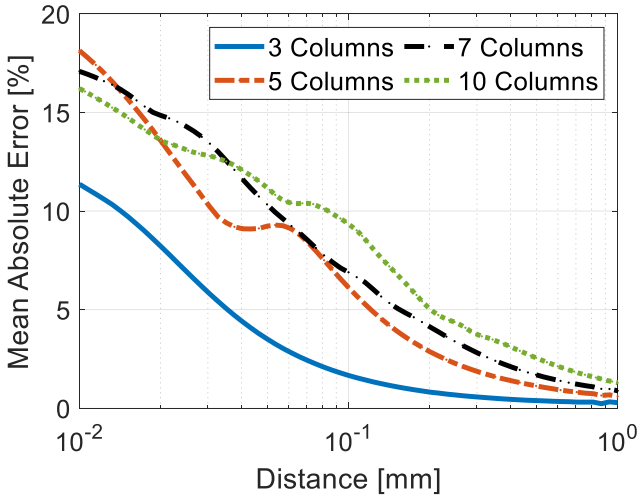

FIGURE 6. **Mean absolute error between the distributed and lumped-parameter models for an array element comprised of different number of columns at different propagation distances. The polarization is kept constant at $V_{DC} = 0.8V_C$.**

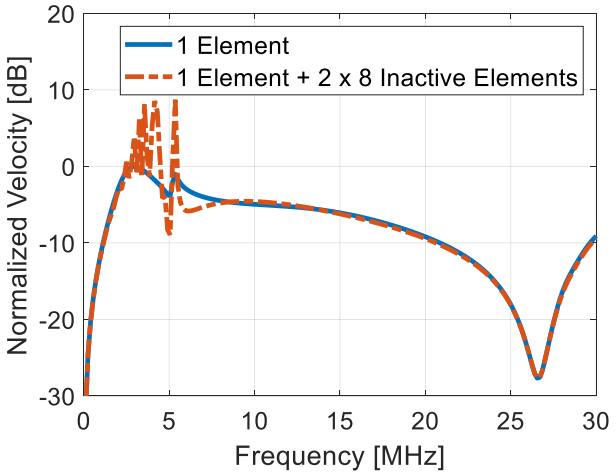

FIGURE 7. **Spatial mean output particular velocity simulation results single isolated CMUT element and a central 1V excited element in an array comprised of 16 inactive neighboring elements ($V_{DC} = 0.8V_C$). All curves are normalized by the maximum velocity of the isolated element (18mm/s).**

element and 16 inactive neighboring elements was simulated. The neighboring elements are biased at $V_{DC} = 0.8V_C$ but not excited. This situation corresponds to the emission of a focused or steered ultrasound beam, where elements are excited one after each other with the suitable delay time. The spatial mean output particular velocity of the excited element placed at the center of the aperture (9^{th} position) is plotted and compared with the response of a single isolated element.

Spurious resonances appear in the frequency response computed with inactive elements. However, as already explained, in a real situation these modes vanish once the probe is encapsulated with a soft polymer, due to viscoelastic effects. In addition, several authors have already observed this phenomenon, pointing out similar conclusions with little influence on the system. As the number of inactive neighboring elements increases, these modes become less visible on the electrical impedance of a device [23], [52] and the emitted pressure field [53], [54]. Hence, for design purposes, considering only one isolated element without inactive neighboring elements remains a valid assumption.

The second case corresponds to array electronic driving conditions used for plane-wave based ultrasonic imaging. This technique relies on the parallel excitation of all elements, to emit plane-waves at different angles. The worst case for the proposed lumped-parameter model is the 0° angle situation since no delay is applied between elements. Simulation results of single element surrounded by 16 active biased and excited elements are compared with the single isolated element, as plotted Fig. 8.

As previously, spurious resonances appear around $4MHz$. Once again, by considering the viscoelasticity of an encapsulation material, the lumped-parameter model will provide the same results as the distributed-element model, with or without neighboring elements after a few propagation wavelengths. Hence for clarity purposes in the remaining sections of this paper, only the single isolated element case will be considered in all simulations.

To summarize, the relevance of the lumped-parameter model was demonstrated for different excitation conditions in line with standard beamforming strategies. The validity limits of our approach were identified. We have shown the lumped-parameter model fails mainly to predict pressure in the near field of the probe, due to crosstalk phenomena between CMUTs. However, it agrees very well with the distributed-element model in the far field area where ultrasound probes are generally exploited. In a real situation, polymer encapsulation natively ensures model validity due to crosstalk reduction linked to viscoelasticity.

B. SIMPLIFIED DEFINITIONS OF THE ACOUSTIC IMPEDANCE TERMS

As seen previously, the two-port network equivalent electroacoustic circuit is comprised of a radiation impedance and a mechanical impedance. The latter corresponds to the energy not dissipated in the fluid, which is absorbed by the mechanical vibrating structure itself. This decomposition follows Mason's analysis but is not always the most suitable tool to investigate the electroacoustic behavior of a CMUT-based (or PMUT-based) array element. It may be more relevant to decompose the acoustic output power into two parts. A part absorbed by the set of CMUTs as if they were acoustically not coupled and another part that corresponds to the collective effects (*i.e.*, the acoustic mutual interactions). To implement this decomposition, the total acoustical power in (6) is written as:

$$\begin{aligned} W_T(\omega) &= W_m(\omega) + W_r(\omega) \\ W_T(\omega) &= \frac{1}{2} N_p [\dot{u}_s]^{T*} [K_m] [\dot{u}_s] \\ &\quad + \frac{1}{2} N_p [\dot{u}_s]^{T*} \left[K_{fluid}\right] [\dot{u}_s] \end{aligned} \tag{16}$$

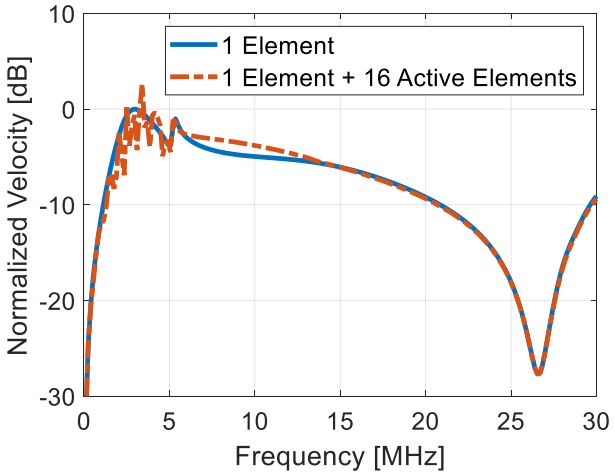

FIGURE 8. Spatial mean output particular velocity simulation results of a single isolated CMUT element and an element in an array comprised of 16 1*V* excited active neighboring elements ($V_{DC} = 0.8V_C$). All curves are normalized by the maximum velocity of the isolated element (18*mm*/*s*).

To extract mutual-acoustic interactions effects, one has just to write $[K_{fluid}]$ as:

$$[K_{fluid}] = \begin{bmatrix} Z_r & \dots & 0 \\ \vdots & \ddots & \vdots \\ 0 & \dots & Z_r \end{bmatrix} + \begin{bmatrix} 0 & \dots & Z_{i,j}^{mut} \\ \vdots & \ddots & \vdots \\ Z_{i,j}^{mut} & \dots & 0 \end{bmatrix}$$
$$[K_{fluid}] = [K_r] + [K_{mut}] \tag{17}$$

$[K_r]$ corresponds to the self-radiation impedance matrix, and $[K_{mut}]$ to the mutual-radiation impedance matrix. From this decomposition, two new impedances terms can be calculated:

$$\begin{cases} Z_{single} = \dfrac{2W_{single}(\omega)}{|\dot{u}_p|^2} \\ Z_{mut} = \dfrac{2W_{mut}(\omega)}{|\dot{u}_p|^2} \end{cases} \tag{18}$$

where Z_{single} is the acoustical impedance of the set of CMUT cells as if they were not acoustically coupled, and Z_{mut} is a global mutual acoustic impedance term that corresponds to the mutual part of the radiated power. W_{single} and W_{mut} are the involved acoustic powers associated with each of the two impedances, respectively defined as:

$$\begin{cases} W_{single}(\omega) = \dfrac{1}{2} N_p [\dot{u}_s]^{T*} [K_m] [\dot{u}_s] \\ + \dfrac{1}{2} N_p [\dot{u}_s]^{T*} [K_r] [\dot{u}_s] \\ W_{mut}(\omega) = \dfrac{1}{2} N_p [\dot{u}_s]^{T*} [K_{mut}] [\dot{u}_s] \end{cases} \tag{19}$$

Classically, one needs to know a specific solution of the distributed-element model $[\dot{u}_s]$ to compute these new impedances. However, another possible choice is to consider a uniform displacement field vector (*i.e.*, all the term are identical) that translates in-phase vibrations of all cells and cancels the visible crosstalk effects. A uniform velocity term $\dot{u}_0$ is defined:

$$\sum_{i=1}^{N_c} \dot{u}_{s,i} = N_c \dot{u}_0 \tag{20}$$

Hence, one can replace the distributed-element model specific solution by the uniform vector that allows easier computation of the impedances. The simplified expression of the equivalent piston velocity given (4) reduces to:

$$\dot{u}_p = \frac{S_{mut}}{S_p} N_p N_c \dot{u}_0 \tag{21}$$

This expression leads to the computation of Z_{single}, which does not depend on the mutual-interactions phenomena, reduced to the following relation:

$$Z_{single} = \frac{Z_m + Z_r}{\left(\frac{S_{mut}}{S_p}\right)^2 N_c N_p} \tag{22}$$

Here, the impedance does not require a specific solution $[\dot{u}_s]$ of the distributed-element model. Indeed, Z_{single} corresponds to the impedance of a single cell with an applied factor that considers the number of cells per element and the active acoustic surface ratio. This term gives clear identification of the central frequency and mechanical cut-off properties of the array-element when the latter is free of mutual coupling effects.

Likewise, the computation of Z_{mut} is greatly simplified since it can be determined without using the distributed-element model. Z_{mut} becomes the mutual acoustic impedance of an array of fluid coupled pistons, for which many solutions are available in the literature [12], [33], [36], [55]. Under these conditions, Z_{mut} yields:

$$Z_{mut} = \frac{\sum_{i=1}^{N_c} \sum_{j=1, j\neq i}^{N_c} Z_{i,j}^{mut}}{\left(\frac{S_{mut}}{S_p} N_c\right)^2 N_p} \tag{23}$$

To assess the relevance of this approach, the distributed element model, the lumped-parameter model, and the lumped-parameter model with uniform displacement field vector are compared. Fig. 9 shows the response of the array element comprised of a single column (solid blue curve), the response where mutual interactions effects are taken into-account, using the classical mechanical Z_{mp}, radiation Z_{rp} impedances decomposition (solid orange curve) and the new single Z_{single} and mutual Z_{mut} impedances decomposition (dotted black curve).

Fig. 9 highlights the significant impact of the mutual interactions on the array element central frequency and bandwidth. Both decompositions give identical results except for the intended disappearance of the crosstalk effects. Moreover, the high cut-off frequency depends only on the CMUT topology and is, as expected, preserved. This means the intrinsic performances of the array element in terms of central frequency, bandwidth, and sensitivity, can be easier assessed with accuracy when the baffle effects are not considered.

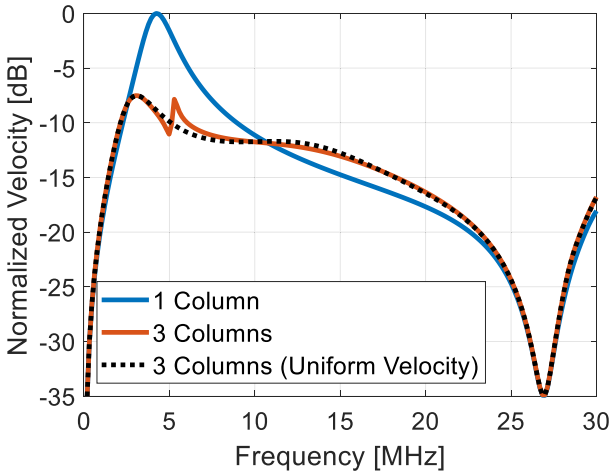

FIGURE 9. Output spatial mean velocity of a single column of CMUTs (solid blue curve), of the array element where mutual interactions are considered, using the classical mechanical Z_{mp}, radiation Z_{rp} impedances decomposition (solid orange curve) and the new single Z_{single} and mutual Z_{mut} impedances decomposition (dotted black curve). All curves are normalized by a maximum velocity of 42 mm/s.

From a practical point of view, the model simplifies greatly the analysis by reducing to a two-computation step process the parameters assessment, one for the equivalent single CMUT parameters (Z_m and Z_r), and one to determine Z_{mut} assuming perfectly stiff piston vibrations. Then, the equivalent lumped parameters of the element are directly obtained from (22) and (23). For the remaining part of the paper, only the model with the new decomposition and no visible crosstalk effects will be used.

C. DEFINITION OF THE RECIPROCAL INPUT/OUTPUT RELATIONSHIPS

As described by Schmerr and Song [43], the possible transfer functions of an acoustic transducer are linked to the following quantities:voltage and current on the electrical port, force and velocity on the acoustical port. This leads to four different possible reciprocal transfer functions, denoted S^{TX} in emission and S^{RX} in reception, with each time a different frequency response and a different unit. However as discussed previously, to ensure consistency with the lumped-parameter model and therefore the distributed-element model, only the output mean velocity must be considered. This reduces the possible transfer functions in emission to:

$$\begin{cases} S^{TX}_{\dot{u}_{ps}V} = \dfrac{\dot{u}_{ps}}{V} \\ S^{TX}_{\dot{u}_{ps}I} = \dfrac{\dot{u}_{ps}}{I} \end{cases} \tag{24}$$

The consistency with the lumped-element model is not the only reason for which these two transfer functions are the most suitable to compute the output electroacoustic response of a transducer. Looking at the basic theory of ultrasonic source radiation [31], [56], [57], there are three possible boundary conditions expressed respectively through the Rayleigh integral: the normal output velocity is null outside the transducer (hard baffle condition), the Rayleigh-Sommerfeld integral (soft baffle condition) and the Kirchhoff integral (free-space boundary condition). In the case of a CMUT-based array element, hard baffle is the most suitable boundary condition since the substrate is considered infinitely hard compared to the mechanical stiffness. In other words, the output velocity of the radiating surface is null outside the radiating element. It is thus appropriate that the particular velocity is the output data exploited to assess the element emission performances.

In reception, it is common practice to construct the equivalent Thevenin or Norton model of the element to account for the electric load conditions. This means that the two electrical quantities of interest are V_{open} which corresponds to the voltage delivered with open-load condition, and I_{short} which is the electrical current delivered using a short-load condition. For each of these quantities, two transfer functions should be defined depending on the input acoustic data, the input spatial mean velocity $\dot{u}_p$ or the input equivalent blocked force F_B. However, the emission-reception performances of the element have to be defined through two transfer functions which meet the electroacoustic reciprocity theorem [29]. This theorem states the absolute emission sensitivity (S^{TX}) to reception sensitivity (S^{RX}) ratio must be homogeneous in terms of unit and equal to one. The two receiving transfer functions to keep are then:

$$\begin{cases} S^{RX}_{VF_B} = \dfrac{V_{open}}{F_B} = \dfrac{V_{open}}{2P_iS_p} \\ S^{RX}_{IF_B} = \dfrac{I_{short}}{F_B} = \dfrac{I_{short}}{2P_iS_p} \end{cases} \tag{25}$$

F_B is the equivalent input force generator associated with an incident plane wave of pressure amplitude P_i. One can show that the emission transfer function $S^{TX}_{\dot{u}_{ps}V}$ unit is $m/s/V$ and matches with the receiving transfer function $S^{RX}_{IF_B}$ unit A/N. Similarly, the $S^{TX}_{\dot{u}_{ps}I}$ transfer function in $m/s/A$ matches with the $S^{RX}_{VF_B}$ unit in V/N. Finally, after a few calculations, the following relation is verified:

$$\left| \frac{S^{RX}_{VF_B}}{S^{TX}_{\dot{u}_pI}} \right| = \left| \frac{S^{RX}_{IF_B}}{S^{TX}_{\dot{u}_pV}} \right| = 1 \tag{26}$$

This result is key to optimize the pulse-echo mode of CMUT arrays. The two reciprocal transfer functions are presented Fig. 10.

The behavior described by the solid orange curve when the output electronic circuit is designed to detect the open-load voltage in reception confirms that it is reciprocal to a current driven emission. Such working conditions are comparable to those of a microphone where the useful frequency band ranges from low frequencies up to the resonance frequency. Above the resonance, the CMUT output capacitance acts as a low-pass filter and decreases the output signal amplitude. Typically, this mode is suitable to work through media where attenuation is strong, and where low frequencies are favored,

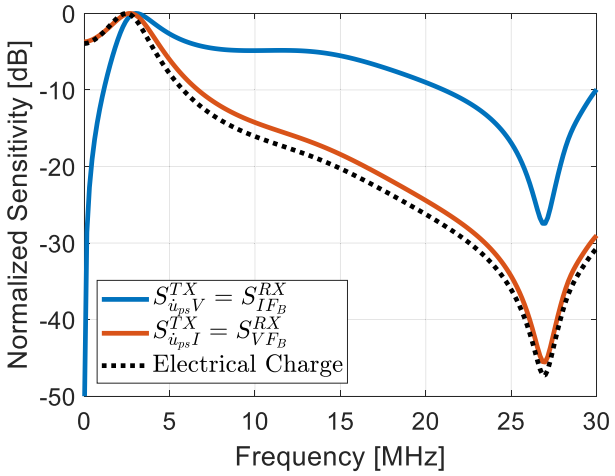

FIGURE 10. Reciprocal sensitivities in transmit and receive modes of a CMUT element and its electrical charge at $V_{DC} = 0.8V_C$. All curves are normalized by their maximum sensitivity values, which are respectively $18mA/N$ for the solid blue curve, $21V/N$ for the solid orange curve, and $1nC/N$ for the dotted black curve.

such as bones [58] or brain imaging/therapy applications where the skull has to be crossed. Note also that the output voltage signal is very close to the output electrical charge signal, as shown by the dotted black curve Fig. 10. This means that in reception, a charge amplifier could also be used to drive the received signals [59].

The behavior described by the solid blue curve when the receiving electronic circuit is designed to detect short-load electrical current shows that the emitter must operate at constant voltage. The response strongly differs from the previous one because the low-pass filtering due to the CMUT capacitance does not affect this transfer function. The high frequency band above the resonance frequency is favored, as well as the relative frequency bandwidth. This situation is often the one retained for CMUT to exploit their performances in terms of bandwidth, as required for harmonic imaging [60] or high-resolution imaging [61]. It is worth mentioning the importance of electrical driving conditions on the performances of the array element. Situations can arise where the transmit and receive transfer functions do not match. Moreover, it is often mentioned in the literature that CMUTs are mainly characterized by a broad frequency bandwidth response. Simulations show that this statement is true only if the current produced by the transducer is sensed.

To close this section, it is interesting to discuss other possible exploitation of the lumped-element representation which, even if evident, provides a clear insight into the parameters that are relevant to the desired application. In addition to the common pulse-echo imaging applications, therapeutic applications [62] and passive acoustic imaging [63], [64] could be addressed specifically. For therapeutic purposes, the output quantity is the mean radiated acoustic power only. The electrical scheme given in Fig. 3, shows that the intrinsic emitter efficiency is governed by the acoustic matching between the Z_{mp} and Z_{rp} impedances which are the two quantities of interest. Indeed, to ensure maximum transmit efficiency at a specific frequency, the sum of both impedances at this working value should be minimal. For passive acoustic imaging, CMUTs are used as a receiver only. Depending on the electronic receiving circuits, a broad range of ultrasonic frequencies can be assessed, ranging from few kilohertz [65] to tens of megahertz [66].

IV. DESIGN RULES OF A CMUT-BASED ARRAY ELEMENT

This last section aims to show how the lumped-parameter model can be used to build design rules of an array element that agrees with a set of initial specifications. For pulse-echo imaging applications, the design of a $\lambda/2$ pitch, $5MHz$ centered array with periodically spaced columns is used as an illustrative example. The method is based on the optimization of the $\left|S^{TX}_{\dot{u}_pV}\right| = \left|S^{RX}_{IF_B}\right|$ transfer function, which implies a constant voltage generator in emission and a broad bandwidth of the transducer's response (cf. Fig. 10). This is the classical ultrasonic imaging pulse-echo setup for CMUT arrays. The tunable inputs are the CMUT-cell topology (membrane thickness and size), the number of cells per element, and the distance between CMUT cells. The outputs are the central frequency, the sensitivity and the $-3dB$ relative frequency bandwidth. The proposed design rules are founded on the separation of the impedance terms of Section III.B (*i.e.*, Z_{single} and Z_{mut}), where the first step is the single CMUT-cell design, and the second step is the full array element design. Only square shape CMUTs will be investigated here.

A. THE IMPACT OF MUTUAL COUPLING ON A SINGLE COLUMN OF CMUTs

To achieve the same central frequency, several element topologies are possible, each providing different performances. It is essential to identify all these configurations to find the optimal design which best meet the specifications. The case of a single column of CMUT cells must be considered first to select all CMUT cell topologies (membrane size and thickness) that are acoustically centered at the chosen central frequency.

Starting from the initial thickness of the Si layer given in Table 1, the targeted device's thickness was swept from $1\mu m$ to $4\mu m$, in line with commercially available SOI thicknesses. Then, for each thickness, the CMUT cell size was adjusted to find the configuration that matches the $5MHz$ central frequency. The electrode thickness was kept to the value given in Table 1. The periodic CMUT-to-CMUT pitch along the element elevation was fixed like previously to $3\mu m$ and the polarization voltage for each configuration is set to $V_{DC} = 0.8V_c$. The obtained results are plotted Fig. 11, giving an initial basis of CMUT cell topologies which can be used to design the array element.

Then, to construct an array element from one of the solutions given Fig. 11, one must gather and spread out

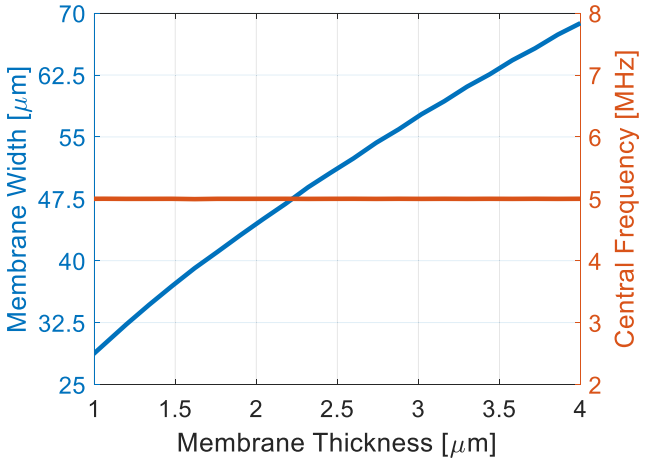

FIGURE 11. Evolution of the thickness-size pairing master curve of CMUTs needed to obtain an immersed central frequency of 5 MHZ when cells are arranged in a single column.

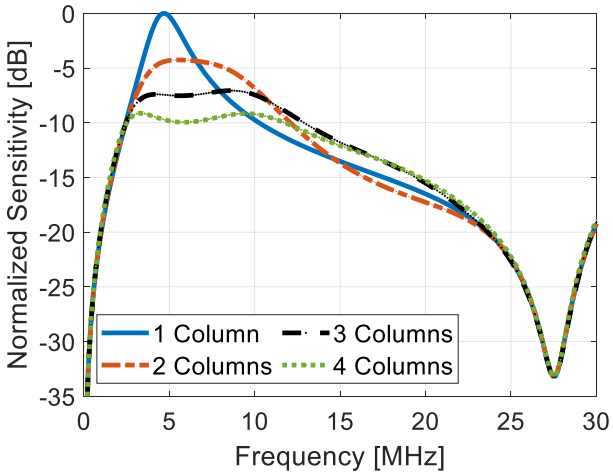

FIGURE 12. $\left|S^{TX}_{\dot{u}_p V}\right| = \left|S^{RX}_{IF_B}\right|$ sensitivity of the single column ($34.5\mu m$ x $34.5\mu m$ membrane size) and an element array made of two, three and four columns with respect to an array pitch of $150\mu m$. All curves are normalized by the maximum value $50mm/s/V$ of the single column configuration.

periodically along the element width several columns of CMUT. Of course, the number of columns per element is limited by the element width and the minimal CMUT-to-CMUT distance which can be manufactured until a chosen minimal value of $3\mu m$. Therefore, a $5MHz$ centered array with a pitch of $\lambda/2$ (*i.e.*, $150\mu m$) sees a maximum of four manufactured columns within its elements. To investigate the impact of increasing number of columns on the central frequency and the frequency bandwidth, the four columns element will be used as the discussion's basis as it gives the maximal active surface given our initial constraints. This specific case corresponds to a membrane size of $34.5\mu m \times 34.5\mu m$. Among the calculated solutions given Fig. 11, the corresponding membrane thickness is $1.33\mu m$. Fig. 12 draws the element sensitivity $\left|S^{TX}_{\dot{u}_p V}\right| = \left|S^{RX}_{IF_B}\right|$ for a single column and the four columns configurations. The intermediate cases of two and three columns element using the same thickness-size pairing were also simulated. The column-to-column pitch was changed to $40.5\mu m$ for the two columns configuration and to $15.5\mu m$ for the three columns element. Indeed, the columns are chosen to remain periodically spread from element-to-element.

Even if the mechanical cut-off frequency is preserved ($27.6MHz$), curves show the significant impact of mutual acoustic coupling on the electroacoustic response of the single CMUT column. The maximum sensitivity of the element is reduced for each column added, which also translates a bandwidth increase. The central frequency appears shifted towards higher frequencies. This shift can be easily explained by looking at the electroacoustic equivalent circuit of the element, given Fig. 3. The resonance occurs when the imaginary parts of Z_{mp} and Z_{rp} have equal amplitude with opposite signs, their summation becomes null.

Looking at Fig. 13, the imaginary part of Z_{mp} and Z_{rp} are drawn for the full array elements. It appears the crossing point shifts from $6MHz$ for the two columns, to $7MHz$ for the array element made of four columns. This shift is due to the imaginary part of the radiation impedance which varies with the mutual impedance term Z_{mut}. Moreover, it is possible to understand the change of the frequency bandwidth through an analysis of the radiation impedance real part. The higher the real part value is, the higher the damping caused by the fluid and therefore the higher the frequency bandwidth.

To conclude this first section, the thickness-size curve determined Fig. 11 without considering the acoustical mutual interactions is not enough to design an array element. For each swept thickness value, the membrane size obtained must be adjusted a second time to restore the central frequency to the targeted value. Of course, this operation must also be repeated for each element configuration.

B. FULL ARRAY ELEMENT DESIGN

The previous analysis was repeated at the element level for all thickness values previously swept (from $1\mu m$ to $4\mu m$), and for the three element configurations. Likewise, each configuration is designed to have periodically spaced columns. It is worth mentioning that the choice of a periodic layout is the most suitable to address all the imaging methods, in particular plane wave techniques [67]. The thickness-size pairs which give an immersed element central frequency of $5MHz$, as well as the required inter-column spaces associated to each pair, are plotted Fig. 14a and Fig. 14b respectively. At the end of all simulations carried out, it appears that for a given thickness, the width of the membrane required to reach the desired frequency is always the same whether for the element is comprised of two, three or four columns. This explains why there is only one curve, and not three as one could initially expect.

The set of points forms a master curve that contains all the configurations matching the desired central frequency for each element. This means that it is possible to get the

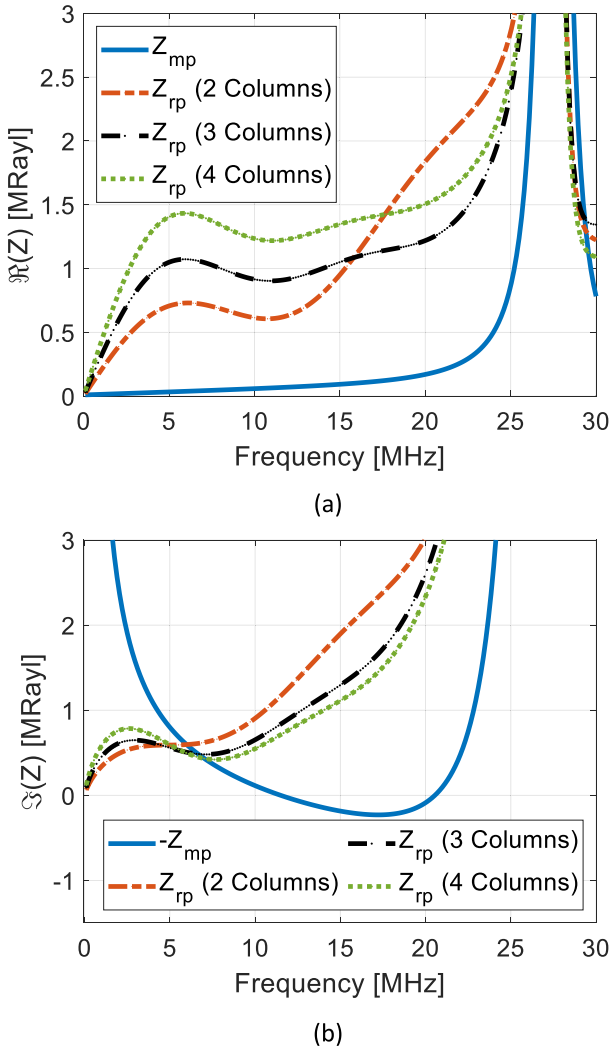

FIGURE 13. **Real part (a) and imaginary part (b) of the mechanical impedance (Z_{mp}) and radiation impedance (Z_{rp}) of a 1-D periodic CMUT array element comprised of 2, 3 and 4 columns. All curves are normalized by the membrane size. The imaginary part of Z_{mp} is multiplied by -1 to see the crossing point with the imaginary part of Z_{rp} (i.e., the frequency for which their summation equals zero).**

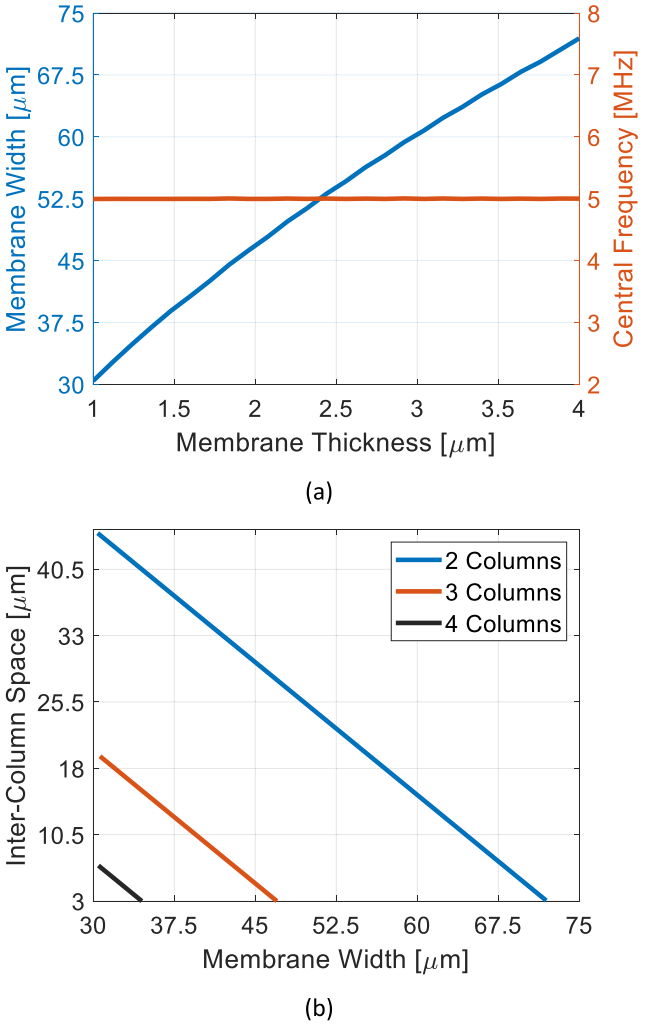

FIGURE 14. **Evolution of the thickness-size pairing master curve of CMUTs (a) needed to obtain an immersed central frequency of 5*MHz* when cells are arranged in a two, three or four columns element. Inter-column space of each array element configurations (b) associated to the thickness-size pairs required to obtain the desired central frequency and the fixed pitch of $\lambda/2$.**

same central frequency using the same membranes size and thickness for array elements having different number of columns. The membrane size range is limited for the three and four columns configurations because the fixed pitch of $\lambda/2$ indirectly sets the inter-CMUT distance which can be manufactured until the chosen minimal value of $3\mu m$. Hence, the results for the three and four columns are defined over a lower range of values than the two columns configuration.

Nevertheless, the central frequency is not enough to define topologies suitable for a given application, sensitivity and bandwidth must also be considered. To complete the design master curve for each of the relevant configurations working at $5MHz$, the $\left|S^{TX}_{\hat{u}_p V}\right| = \left|S^{RX}_{IF_B}\right|$ sensitivity curves were post-processed to extract their maximum values and the $-3dB$ relative frequency bandwidth. The results are plotted Fig. 15. Only the thickness is displayed on the abscissa axis, but each thickness value is associated a specific membrane width and inter-cell space in accordance with the master curves presented Fig. 14. Hence, for each result, three variables are considered regarding CMUT cell geometries and array element design.

A clear difference exists between each configuration, especially the one comprised of two columns and the two others. First, in terms of sensitivity, a loss of almost $4dB$ can be observed between the two columns and the four columns configurations at the expense of the frequency bandwidth. Each configuration achieves naturally more than 100% of bandwidth, a standard value for classical imaging applications. Note that for the two columns element the maximal bandwidth is reached around a $2.5\mu m$ thick membrane with no further major improvements on the sensitivity using thicker

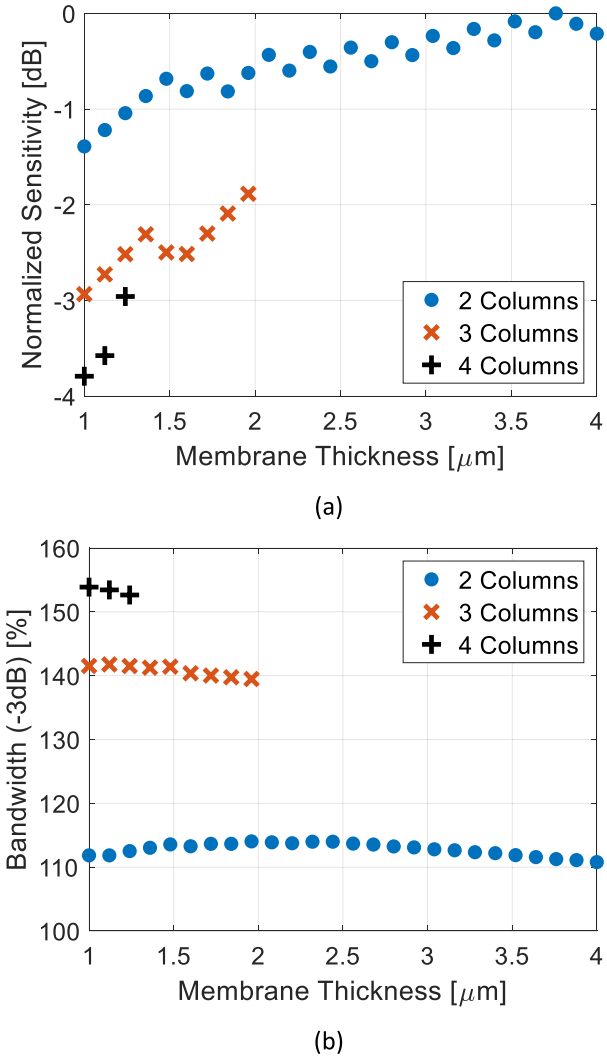

FIGURE 15. Performance values for the set of array element configurations defined Fig. 14. Each configuration delivers the same central frequency (5*MHz*) for the same array pitch ($\lambda/2$, 150μm). Every value displayed is associated to *a* specific membrane width, thickness, and inter-cell space. Sensitivities (*a*) are plotted using membrane thickness normalized by *a* maximum value of 16*mm*/*s*/*V*. In the same manner, −3*dB* relative frequency bandwidth values (*b*) are plotted using membrane thickness.

membranes. Thus, it is not necessary to increase membrane thickness for this device above 2.5μm.

The three and four columns configurations are very similar in terms of performances. A bandwidth of 140% is achieved with the three columns element, outperformed by the 155% of the 4 columns element, but with a lower sensitivity. The bandwidth is constant over the complete thickness range between 1μm and 2μm, meaning that using our constraints, thicker membranes do not improve bandwidth. However, thicker membranes can benefit from a 1dB sensitivity gain. Keep in mind that for a pulse-echo operating mode, each of the plotted sensitivity value must be multiplied by two to consider the complete measurement chain. Therefore, the 3 columns element comprised of 46μm × 46μm × 2μm membranes seems to be the best trade-off for the ultrasonic imaging application targeted here.

If a second device with a different central frequency must be designed on the same wafer, the same analysis can be carried. Hence, the set of curves given Fig. 14 and Fig. 15 become essential to select a material thickness that is best suited to all the applications targeted. In other words, it is fundamental to scan all possible thickness-size pairs, to be able to associate several configurations on the same wafer and to identify performances trade-offs of the probe, in terms of sensitivity and/or bandwidth.

V. CONCLUSION

This paper demonstrated the relevance of the simulation scale change for CMUT-based array element from the unit cell to the full array element. A new model of CMUT population using an equivalent lumped-parameter circuit was implemented. It allows the input/output relationships of an array element to be expressed through a standard two-port network circuit. This operation reduces the number of degrees of freedom while maintaining the accuracy of the simulations. Based on Foldy's analysis which defines the acoustic impedance from acoustic power balance equations, a new set of acoustic impedance terms to model the CMUTs-fluid coupling was introduced. It was proposed to separate the total output acoustic power as the sum of two parts, one that corresponds to the self-acoustic power of each CMUT and another that corresponds to the mutual-acoustic power between each CMUT. Assuming each CMUT vibrate as perfect rigid pistons, the mutual-acoustic power computation is drastically simplified, and does not require any numerical solving tools such as finite element or finite differences.

To further emphasize the lumped-parameter model efficiency, a reciprocity analysis was led. Two main transfer functions for CMUT-based array elements that ought to be considered for the desired application were identified. Mindful considerations are required while considering the reception measurement chain and especially the electrical loading impedance, which can greatly impact the transducer response.

Finally, based on the developed model, a methodology was proposed to help in the CMUT design. Given all the parameters that need to be adjusted, the most important step is to find all the configurations that meet the targeted central frequency. It is recommended to do this in two steps, considering only the self-acoustic power and then adding the mutual-acoustic power. This provides a set of master curves from which are selected the most efficient configurations in terms of sensitivity or bandwidth. One possible extension of this work is to apply the model to the design of 2D arrays and link it with ultrasound image simulation models.

REFERENCES

[1] M. I. Haller and B. T. Khuri-Yakub, "A surface micromachined electrostatic ultrasonic air transducer," *IEEE Trans. Ultrason., Ferroelectr., Freq. Control*, vol. 43, no. 1, pp. 1–6, Jan. 1996.

[2] I. Ladabaum, X. Jin, H. T. Soh, A. Atalar, and B. T. Khuri-Yakub, "Surface micromachined capacitive ultrasonic transducers," *IEEE Trans. Ultrason., Ferroelectr., Freq. Control*, vol. 45, no. 3, pp. 678–690, May 1998.

[3] A. Lohfink and P.-C. Eccardt, "Linear and nonlinear equivalent circuit modeling of CMUTs," *IEEE Trans. Ultrason., Ferroelectr., Freq. Control*, vol. 52, no. 12, pp. 2163–2172, Dec. 2005.

[4] K. Brenner, A. S. Ergun, K. Firouzi, M. F. Rasmussen, Q. Stedman, and B. Khuri-Yakub, "Advances in capacitive micromachined ultrasonic transducers," *Micromachines*, vol. 10, no. 2, p. 152, 2019.

[5] U. Demirci, A. S. Ergun, O. Oralkan, M. Karaman, and B. T. Khuri-Yakub, "Forward-viewing CMUT arrays for medical imaging," *IEEE Trans. Ultrason., Ferroelectr., Freq. Control*, vol. 51, no. 7, pp. 887–895, Jul. 2004.

[6] A. S. Savoia, G. Caliano, and M. Pappalardo, "A CMUT probe for medical ultrasonography: From microfabrication to system integration," *IEEE Trans. Ultrason., Ferroelectr., Freq. Control*, vol. 59, no. 6, pp. 1127–1138, Jun. 2012.

[7] S. Park *et al.*, "CMUT-based resonant gas sensor array for VOC detection with low operating voltage," *Sens. Actuators B, Chem.*, vol. 273, pp. 1556–1563, Nov. 2018.

[8] P. Shanmugam *et al.*, "Broad bandwidth air-coupled micromachined ultrasonic transducers for gas sensing," *Ultrasonics*, vol. 114, Jul. 2021, Art. no. 106410.

[9] K. Chen, H.-S. Lee, and C. G. Sodini, "A column-row-parallel ASIC architecture for 3-D portable medical ultrasonic imaging," *IEEE J. Solid-State Circuits*, vol. 51, no. 3, pp. 738–751, Mar. 2016.

[10] G. Gurun, P. Hasler, and F. L. Degertekin, "Front-end receiver electronics for high-frequency monolithic CMUT-on-CMOS imaging arrays," *IEEE Trans. Ultrason., Ferroelectr., Freq. Control*, vol. 58, no. 8, pp. 1658–1668, Aug. 2011.

[11] G. Gurun *et al.*, "Single-chip CMUT-on-CMOS front-end system for real-time volumetric IVUS and ICE imaging," *IEEE Trans. Ultrason., Ferroelectr., Freq. Control*, vol. 61, no. 2, pp. 239–250, Feb. 2014.

[12] M. Maadi and R. J. Zemp, "Self and mutual radiation impedances for modeling of multi-frequency CMUT arrays," *IEEE Trans. Ultrason., Ferroelectr., Freq. Control*, vol. 63, no. 9, pp. 1441–1454, Sep. 2016.

[13] Y. Qiu *et al.*, "Piezoelectric micromachined ultrasound transducer (PMUT) arrays for integrated sensing, actuation and imaging," *Sensors*, vol. 15, no. 4, pp. 8020–8041, 2015.

[14] T. Xu *et al.*, "Array design of piezoelectric micromachined ultrasonic transducers with low-crosstalk and high-emission performance," *IEEE Trans. Ultrason., Ferroelectr., Freq. Control*, vol. 67, no. 4, pp. 789–800, Apr. 2020.

[15] I. O. Wygant, M. Kupnik, and B. T. Khuri-Yakub, "Analytically calculating membrane displacement and the equivalent circuit model of a circular CMUT cell," in *Proc. IEEE Ultrason. Symp.*, Nov. 2008, pp. 2111–2114.

[16] H. K. Oguz *et al.*, "Nonlinear modeling of an immersed transmitting capacitive micromachined ultrasonic transducer for harmonic balance analysis," *IEEE Trans. Ultrason., Ferroelectr., Freq. Control*, vol. 57, no. 2, pp. 438–447, Feb. 2010.

[17] M. Maadi and R. J. Zemp, "A nonlinear lumped equivalent circuit model for a single uncollapsed square CMUT cell," *IEEE Trans. Ultrason., Ferroelectr., Freq. Control*, vol. 66, no. 8, pp. 1340–1351, Aug. 2019.

[18] K. Smyth and S.-G. Kim, "Experiment and simulation validated analytical equivalent circuit model for piezoelectric micromachined ultrasonic transducers," *IEEE Trans. Ultrason., Ferroelectr., Freq. Control*, vol. 62, no. 4, pp. 744–765, Apr. 2015.

[19] I. O. Wygant, M. Kupnik, and B. T. Khuri-Yakub, "An analytical model for capacitive pressure transducers with circular geometry," *J. Microelectromech. Syst.*, vol. 27, no. 3, pp. 448–456, Jun. 2018.

[20] S. Satir and F. L. Degertekin, "A nonlinear lumped model for ultrasound systems using CMUT arrays," *IEEE Trans. Ultrason., Ferroelectr., Freq. Control*, vol. 62, no. 10, pp. 1865–1879, Oct. 2015.

[21] H. Köymen *et al.*, "An improved lumped element nonlinear circuit model for a circular CMUT cell," *IEEE Trans. Ultrason., Ferroelectr., Freq. Control*, vol. 59, no. 8, pp. 1791–1799, Aug. 2012.

[22] E. Aydoğdu, A. Ozgurluk, A. Atalar, and H. Köymen, "Parametric nonlinear lumped element model for circular CMUTs in collapsed mode," *IEEE Trans. Ultrason., Ferroelectr., Freq. Control*, vol. 61, no. 1, pp. 173–181, Jan. 2014.

[23] A. Atalar, H. Köymen, and H. K. Oğuz, "Rayleigh–Bloch waves in CMUT arrays," *IEEE Trans. Ultrason., Ferroelectr., Freq. Control*, vol. 61, no. 12, pp. 2139–2148, Dec. 2014.

[24] A. Caronti, A. Savoia, G. Caliano, and M. Pappalardo, "Acoustic coupling in capacitive microfabricated ultrasonic transducers: Modeling and experiments," *IEEE Trans. Ultrason., Ferroelectr., Freq. Control*, vol. 52, no. 12, pp. 2220–2234, Dec. 2005.

[25] C. Meynier, F. Teston, and D. Certon, "A multiscale model for array of capacitive micromachined ultrasonic transducers," *J. Acoust. Soc. Amer.*, vol. 128, no. 5, pp. 2549–2561, 2010.

[26] B. Bayram *et al.*, "Finite element modeling and experimental characterization of crosstalk in 1-D CMUT arrays," *IEEE Trans. Ultrason., Ferroelectr., Freq. Control*, vol. 54, no. 2, pp. 418–430, Feb. 2007.

[27] A. S. Savoia, G. Scaglione, and B. Haider, "Combined use of finite element and equivalent circuit modeling for system-level simulation of integrated capacitive micromachined ultrasonic transducers (CMUT)," in *Proc. IEEE Int. Ultrason. Symp. (IUS)*, Sep. 2020, pp. 1–4.

[28] D. Certon, F. Teston, and F. Patat, "A finite difference model for cMUT devices," *IEEE Trans. Ultrason., Ferroelectr., Freq. Control*, vol. 52, no. 12, pp. 2199–2210, Dec. 2005.

[29] L. L. Foldy, "Theory of passive linear electroacoustic transducers with fixed velocity distribution," *J. Acoust. Soc. Amer.*, vol. 21, no. 6, pp. 595–604, Nov. 1949.

[30] M. Saadatmand and J. Kook, "Differences between plate theory and lumped element model in electrostatic analysis of one-sided and two-sided CMUTs with circular microplates," *J. Brazilian Soc. Mech. Sci. Eng.*, vol. 42, no. 9, p. 468, Sep. 2020.

[31] J. L. Butler and C. H. Sherman, *Transducers and Arrays for Underwater Sound*. Cham, Switzerland: Springer, 2016.

[32] A. Boulme, D. Certon, N. Senegond, C. Meynier, and F. Teston, "A strategy to predict and reduce baffle effects in linear array of CMUTs," in *Proc. IEEE Int. Ultrason. Symp.*, Oct. 2010, pp. 1873–1876.

[33] R. L. Pritchard, "Mutual acoustic impedance between radiators in an infinite rigid plane," *J. Acoust. Soc. Amer.*, vol. 32, no. 6, pp. 730–737, Feb. 1960.

[34] D. T. Porter, "Self- and mutual-radiation impedance and beam patterns for flexural disks in a rigid plane," *J. Acoust. Soc. Amer.*, vol. 36, no. 6, pp. 1154–1161, Jun. 1964.

[35] B. Shieh, K. G. Sabra, and F. L. Degertekin, "Efficient broadband simulation of fluid-structure coupling for membrane-type acoustic transducer arrays using the multilevel fast multipole algorithm," *IEEE Trans. Ultrason., Ferroelectr., Freq. Control*, vol. 63, no. 11, pp. 1967–1979, Nov. 2016.

[36] H. Oguz, A. Atalar, and H. Koymen, "Equivalent circuit-based analysis of CMUT cell dynamics in arrays," *IEEE Trans. Ultrason., Ferroelectr., Freq. Control*, vol. 60, no. 5, pp. 1016–1024, May 2013.

[37] S. Ballandras, M. Wilm, W. Daniau, A. Reinhardt, V. Laude, and R. Armati, "Periodic finite element/boundary element modeling of capacitive micromachined ultrasonic transducers," *J. Appl. Phys.*, vol. 97, no. 3, 2005, Art. no. 034901.

[38] A. Boulmé and D. Certon, "Design of broadband linear micromachined ultrasonic transducer arrays by means of boundary element method coupled with normal mode theory," *IEEE Trans. Ultrason., Ferroelectr., Freq. Control*, vol. 62, no. 9, pp. 1704–1716, Sep. 2015.

[39] B. Shieh, K. G. Sabra, and F. L. Degertekin, "A hybrid boundary element model for simulation and optimization of large piezoelectric micromachined ultrasonic transducer arrays," *IEEE Trans. Ultrason., Ferroelectr., Freq. Control*, vol. 65, no. 1, pp. 50–59, Jan. 2018.

[40] J. A. Jensen, "Field: A program for simulating ultrasound systems," in *Proc. 10th Nordicbaltic Conf. Biomed. Imag.*, vol. 4, 1996, pp. 351–353.

[41] F. Lingvall, "Time-domain reconstruction methods for ultrasonic array imaging: A statistical approach," Uppsala Univ., Uppsala, Sweden, Tech. Rep., 2004.

[42] N. Sénégond, A. Boulmé, C. Plag, F. Teston, and D. Certon, "Fast time-domain modeling of fluid-coupled cMUT cells: From the single cell to the 1-D linear array element," *IEEE Trans. Ultrason., Ferroelectr., Freq. Control*, vol. 60, no. 7, pp. 1505–1518, Jul. 2013.

[43] L. W. Schmerr and S.-J. Song, *Ultrasonic Nondestructive Evaluation Systems: Models and Measurements*. Boston, MA, USA: Springer, 2007.

[44] A. S. Erguri, Y. Huang, X. Zhuang, Ö. Oralkan, G. G. Yaraholu, and B. T. Khuri-Yakub, "Capacitive micromachined ultrasonic transducers: Fabrication technology," *IEEE Trans. Ultrason., Ferroelectr., Freq. Control*, vol. 52, no. 12, pp. 2242–2258, Dec. 2005.

[45] F. Sammoura, K. Smyth, and S.-G. Kim, "An equivalent network representation of a clamped bimorph piezoelectric micromachined ultrasonic transducer with circular and annular electrodes using matrix manipulation techniques," *IEEE Trans. Ultrason., Ferroelectr., Freq. Control*, vol. 60, no. 9, pp. 1989–2003, Sep. 2013.
[46] T. Xu *et al.*, "Equivalent circuit model for a large array of coupled piezoelectric micromachined ultrasonic transducers with high emission performance," *IEEE Trans. Ultrason., Ferroelectr., Freq. Control*, vol. 68, no. 3, pp. 718–733, Mar. 2021.
[47] D. Gross, M. Legros, P. Vince, and D. Certon, "Evaluation of an ultrasound-guided focused ultrasound CMUT probe for targeted therapy applications," *Open J. Appl. Sci.*, vol. 8, no. 1, pp. 25–45, 2018.
[48] M. Hery *et al.*, "Broadband vs. sensitive CMUT linear array: A comparative study from bare chip up to image," in *Proc. IEEE Int. Ultrason. Symp. (IUS)*, Oct. 2018, pp. 1–4.
[49] A. Rønnekleiv, "CMUT array modeling through free acoustic CMUT modes and analysis of the fluid CMUT interface through Fourier transform methods," *IEEE Trans. Ultrason., Ferroelectr., Freq. Control*, vol. 52, no. 12, pp. 2173–2184, Dec. 2005.
[50] M. Hery, N. Senegond, and D. Certon, "A boundary element model for CMUT-arrays loaded by a viscoelastic medium," *IEEE Trans. Ultrason., Ferroelectr., Freq. Control*, vol. 67, no. 4, pp. 779–788, Apr. 2020.
[51] T. Merrien, M. Hery, A. Boulme, and D. Certon, "Viscoelasticity assessment using quartz crystal microbalance for accurate loaded CMUT modeling," in *Proc. IEEE Int. Ultrason. Symp. (IUS)*, Sep. 2021, pp. 1–4.
[52] A. Boulme, D. Gross, M. Legros, and D. Certon, "Electroacoustic response of cMUT-based linear arrays: Role of inactive elements," in *Proc. IEEE Int. Ultrason. Symp.*, Sep. 2014, pp. 2599–2602.
[53] M. Pappalardo, A. Caronti, C. Longo, A. Savoia, P. Gatta, and G. Caliano, "Analysis of acoustic interaction effects and crosstalk in CMUT linear arrays for medical imaging," in *Proc. IEEE Ultrason. Symp.*, Oct. 2006, pp. 582–585.
[54] A. Zeshan, X. Zhang, O. Oralkan, and F. Y. Yamaner, "2D CMUT array based ultrasonic micromanipulation platform," in *Proc. IEEE Int. Ultrason. Symp. (IUS)*, Sep. 2016, pp. 1–4.
[55] A. Bozkurt, "A lumped-circuit model for the radiation impedance of a circular piston in a rigid baffle," *IEEE Trans. Ultrason., Ferroelectr., Freq. Control*, vol. 55, no. 9, pp. 2046–2052, Sep. 2008.
[56] G. S. Kino, *Acoustic Waves: Devices, Imaging, and Analog Signal Processing*. Englewood Cliffs, NJ, USA: Prentice-Hall, 1987.
[57] J. Cheeke, *Fundamentals and Applications of Ultrasonic Waves*, vol. 56, no. 4. Boca Raton, FL, USA: CRC Press, 2002.
[58] A. Boulmé *et al.*, "A capacitive micromachined ultrasonic transducer probe for assessment of cortical bone," *IEEE Trans. Ultrason., Ferroelectr., Freq. Control*, vol. 61, no. 4, pp. 710–723, Apr. 2014.
[59] S. Y. Peng, M. S. Qureshi, P. E. Hasler, A. Basu, and F. L. Degertekin, "A charge-based low-power high-SNR capacitive sensing interface circuit," *IEEE Trans. Circuits Syst. I, Reg. Papers*, vol. 55, no. 7, pp. 1863–1872, Aug. 2008.
[60] M. Legros, A. Novell, A. Bouakaz, G. Ferin, R. Dufait, and D. Certon, "Tissue harmonic imaging with CMUTs," in *Proc. IEEE Int. Ultrason. Symp.*, Oct. 2011, pp. 2249–2252.
[61] O. Oralkan, S. T. Hansen, B. Bayram, G. G. Yaralglu, A. S. Ergun, and B. T. Khuri-Yakub, "High-frequency CMUT arrays for high-resolution medical imaging," in *Proc. IEEE Ultrason. Symp.*, Aug. 2004, pp. 399–402.
[62] C. R. Bawiec, W. A. N'Djin, G. Bouchoux, N. Sénégond, N. Guillen, and J.-Y. Chapelon, "Preliminary investigation of a 64-element capacitive micromachined ultrasound transducer (CMUT) annular array designed for high intensity focused ultrasound (HIFU)," *IRBM*, vol. 39, no. 5, pp. 295–306, Nov. 2018.
[63] A. Dauba *et al.*, "Evaluation of capacitive micromachined ultrasonic transducers for passive monitoring of microbubble-assisted ultrasound therapies," *J. Acoust. Soc. Amer.*, vol. 148, no. 4, pp. 2248–2255, Oct. 2020.
[64] R. Manwar, K. Kratkiewicz, and K. Avanaki, "Overview of ultrasound detection technologies for photoacoustic imaging," *Micromachines*, vol. 11, no. 7, p. 692, Jul. 2020.
[65] A. Unlugedik, A. S. Taşdelen, A. Atalar, and H. Köymen, "Designing transmitting CMUT cells for airborne applications," *IEEE Trans. Ultrason., Ferroelectr., Freq. Control*, vol. 61, no. 11, pp. 1899–1910, Nov. 2014.
[66] S. Zhuang, D. Zhao, L. Chen, and L. Zhai, "A 50-MHz CMUT probe for medical ultrasound imaging," in *Proc. IEEE Int. Ultrason. Symp. (IUS)*, Oct. 2018, pp. 1–4.
[67] E. F. Arkan and F. L. Degertekin, "Analysis and design of high-frequency 1-D CMUT imaging arrays in noncollapsed mode," *IEEE Trans. Ultrason., Ferroelectr., Freq. Control*, vol. 66, no. 2, pp. 382–393, Feb. 2019.

TONY MERRIEN was born in Rennes, France, in 1994. He received the M.Sc. degree in physical acoustics from the École Centrale de Lyon, France, in 2018. He is currently pursuing the Ph.D. degree in electrical engineering with the GREMAN UMR-CNRS 7347 Laboratory, in partnership with MODULEUS SAS. His current research focuses on row-column addressed (RCA) capacitive micromachined ultrasonic transducers (CMUT) integration for 3D imaging.

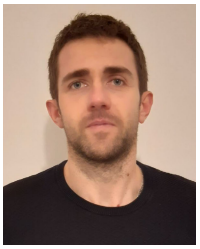

AUDREN BOULMÉ was born in France, in 1987. He received the M.Sc. degree in medical imaging technology from the François Rabelais University of Tours, France, in 2009, and the Ph.D. degree in engineering physics from the University of Tours, France, in 2013. In 2017, he joined MODULEUS SAS as an Research and Development Engineer. His research focuses on modeling, design, and characterization of capacitive micromachined ultrasonic transducers (CMUT).

DOMINIQUE CERTON (Member, IEEE) received the M.Sc. degree in signal processing and electrical engineering in 1991 from the University of Orléans, France, the Ph.D. degree from the University of Tours, France, in 1994, and the Habilitation à Diriger les Recherches (H.D.R.) degree in applied acoustics and materials engineering from the University of Tours in 2006.

He is currently a Full Professor affiliated with the GREMAN Laboratory (UMR-CNRS 7347-University of Tours). In addition to the research activities, he is currently in charge of coordinating the Electronics and Energy Department with the Polytech Tours Engineering School. From more than ten years ago, he developed strong know-how in the design, modeling, and characterization of MEMS-based ultrasonic transducer, i.e. capacitive micromachined ultrasonic transducers (CMUT). He also has over ten years of research experience with multi-element probes based on piezoelectric materials and more specifically with piezo-composite materials. He has been involved in several national and international research projects and has coordinated national research projects funded by the French National Research Agency. A large part of its activities has led to strong industrial collaborations and the transfer of know-how. This relationship with industry has enabled the development of tools for modeling multi-element ultrasound probes that are now used and exploited by some of its industrial partners. He has authored or coauthored more than 60 communications and publications. His research activities focus on ultrasonic probes and related instrumentation applied to medical imaging, and non destructive testing and metrology.

Dr. Certon is a member of the French Society of Acoustics and the IEEE Society.